Materialia 15 (2021) 101042

Contents lists available at ScienceDirect

Materialia

journal homepage: www.elsevier.com/locate/mtla

Full Length Article

On the mechanism of cross-slip induced dislocation substructure formation in an high-Mn steel

S.R. Das[a], S. Shyamal[a], T. Sahu[b], J.I. Kömi[c], P.C. Chakraborti[d], D.A. Porter[c], L.P. Karjalainen[c], P. Sahu[a,*]

[a] Department of Physics, Jadavpur University, Kolkata 700 032, India
[b] Department of Physics, S.A. Jaipuria College, Kolkata 700 005, India
[c] Centre for Advanced Steels Research, University of Oulu, Box 4200, FIN–90014, Finland
[d] Department of Metallurgical and Material Engineering, Jadavpur University, Kolkata 700 032, India

ARTICLE INFO

Keywords:
High-Mn steels
Transmission electron microscopy
Dislocation
Cross-slip
Stacking fault energy

ABSTRACT

The underlying mechanism of dislocation substructure formation in a tensile deformed fine-grained high-Mn steel is reported using transmission electron microscopy. A cross-slip assisted dislocation truncation mechanism was revealed that formed strings of dislocation loops at early strain, which were also retained at fracture strain. Planar glide producing a Taylor lattice was also observed. The dislocation plasticity based on a cross-slip based mechanism delayed dynamic recovery in stage C to manifest an uniform strain hardening. Such a mechanism producing good combination of high strength and ductility is observed for the first time in high-Mn steel.

The paradigm of strain hardening in high-Mn steels revolves around various contributions from deformation twinning, until some recent articles have indicated the importance of dislocation plasticity in these steels [1–3]. Kim and De Cooman [4] have recently suggested that the twinning is suppressed, and dislocation plasticity is enhanced when the stacking fault energy (SFE) exceeds ~ 40 mJ/m^2. The addition of Al increases the SFE of austenite in high-Mn steels, resulting in the suppression of twinning [5]. SFE is also increased and twinning in these steels defeated by deforming above ambient temperature [1]. Though the fundamental reasons remain unclear, austenite grain refinement is also reported to raise SFE [5–8].

When SFE is high, plastic deformation primarily occurs through dislocation glide [9,10] and easy cross-slip, wherein the screw dislocation segments change their glide planes causing what is known as 'wavy glide' [11]. Cross-slip eases dislocation annihilation, *i.e.* dynamic recovery, which reduces the rate of strain hardening due to a reduction in the rate of increase in dislocation density [12]. The literature emphasizing the role of dislocation plasticity over twinning in high-Mn steels claims that the primary deformation mode is the formation of complex substructures induced by cross-slip [2,3]. However, the actual mechanisms engendering the dislocation substructure formation in high-Mn steels are still lacking [13]. In this work, we aim to clarify the mechanism underlying the dislocation movements that produce cross-slip induced dislocation plasticity in a fine-grained high-Mn steel. The objective was to provide fundamental insights into the mechanism of dislocation plasticity in high-Mn steels, reported in the literature [1-3]. A fine grain size was purposely chosen based on the understanding that it suppresses deformation twinning [1,14], and therefore the plasticity would be predominantly dislocation mediated.

A high-Mn steel with the composition (in wt.%) Fe-26Mn-1Al-0.14C was induction-cast, followed by homogenization and hot rolling to an 8 mm strip at 1100 °C and water quenched. It was then cold rolled to a 50% reduction, followed by a recrystallization heat treatment under protective Ar atmosphere at 700 °C for 30 min, and subsequent water quenching to room temperature (RT). The initial microstructure was studied using electron backscatter diffraction (EBSD) in a Hitachi SU7000 ultra high-resolution scanning electron microscope at 20 kV, 6 nA. Uniaxial tensile tests were carried out using A30 specimens (gauge length: 30 mm) in a Zwick Z 100 tensile testing machine at RT with quasi static strain rate of 10^{-4} s^{-1}. The quasi static strain rate was chosen to minimize the scope of SFE alteration during deformation through adiabatic heating. The tensile tests were interrupted at 2%, 5% and 10% true strains to identify the early dislocation activity and also continued until failure occurring at ~ 50% true strain. The deformed gauge regions were used for X-ray diffraction (XRD) investigations (Bruker D8 Advance, CuK_α) in the Bragg–Brentano geometry. Transmission electron microscopy (TEM) observations were carried out on JEOL 2200FS TEM operating at 200 kV.

The thermomechanical treatments described above produced an average grain size ~ 5 μm, measured from the grain size distribution presented as inset to the EBSD inverse pole figure (IPF) map in Fig. 1(a). The

* Corresponding author.
E-mail addresses: psahu74@gmail.com, psahu@phys.jdvu.ac.in (P. Sahu).

https://doi.org/10.1016/j.mtla.2021.101042
Received 14 November 2020; Accepted 21 February 2021
Available online 24 February 2021

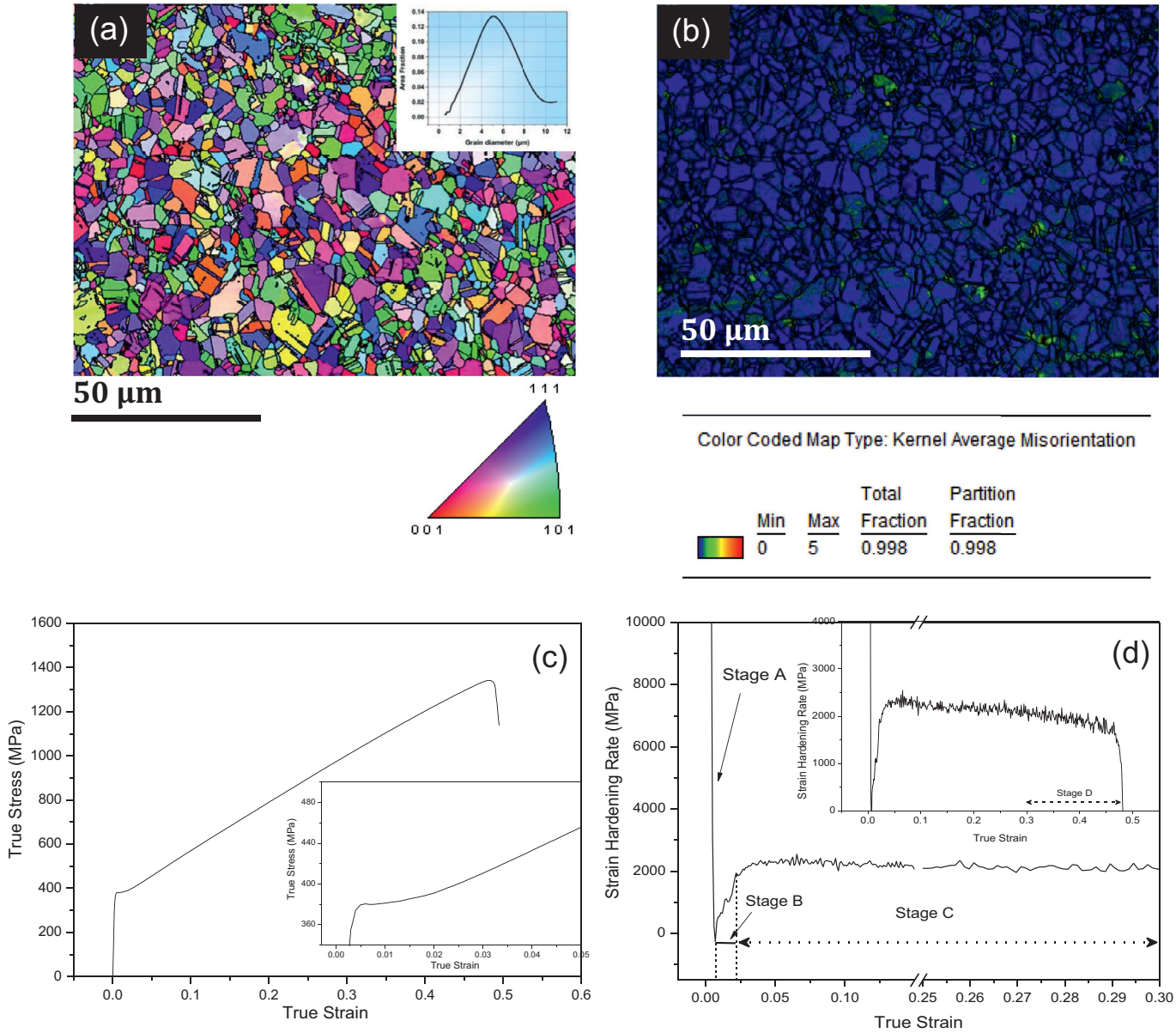

Fig. 1. (a) EBSD IPF map of the initial recrystallized microstructure. (b) KAM map corresponding to (a). (c) True stress – true strain curve of the steel. (d) Strain hardening response of the steel.

corresponding Kernel Average Misorientation (KAM) map in Fig. 1(b) indicates that the specimen is in fully recrystallized condition. The true flow stress curve of the steel is plotted in Fig. 1(c), revealing that the steel had a high final true stress of ~ 1.4 GPa) and fracture strain of ~ 50%, while the absence of serrations in the flow curve ruled out dynamic strain aging (DSA). It can also be seen from the inset in Fig. 1(c) that the flow curve is associated with short discontinuous yielding extending until ~ 2% strain, which is interpreted by Kim and De Cooman [4] as Lüders strain in TWIP steels.

The strain hardening rate (SHR) of the steel is further shown in Fig. 1(d). A critical look at Fig. 1(d) reveals some interesting findings, namely, the transition from stage A to stage B does not exhibit any distinct plateau region, as is often observed for low-carbon high-Mn steels [5]. The present steel in stage B shows an increasing SHR until the beginning of the constant SHR region at a level of ~ 2 GPa in stage C. The maximum in the SHR of low-carbon high-Mn steels is known to occur at the onset of stage C [5]. Usually in stage C, the SHR of high-Mn steels gradually weakens at higher strains, attributed to the difficulty in creating new twins at high strain levels [5]. The nearly constant SHR seen here is typically observed in stage D, due either to the formation of secondary twins and/or twin-twin interactions that restrain dislocation glide [5]. In the present study, the inset in Fig. 1(d) reveals a moderate drop of SHR in stage D. The steel thus reveals a distinct four-stage strain hardening; unlike the interstitial containing high-Mn steels exhibiting five-stage strain hardening (A, B, C, D and E) [15,16], although exceptions are also reported [16].

The specimens were tilted to ⟨110⟩ and ⟨111⟩ zone axes to identify the early dislocation activities, and the associated contrast of the dislocations in a few grains containing lower densities of defects is interpreted according to the modified two-beam dynamical theory of electron diffraction [17], and adopted in our previous studies [18,19]. Fig. 2 shows a set of high magnification micrographs of the 2% deformed specimen acquired along $B \approx [111]$, revealing the activation of multiple slip and interaction among different $\frac{a}{2}\langle 110\rangle$ dislocations on the {111} planes. The bright field (BF) image in Fig. 2(a) demonstrates the first case, where the impingement between $\frac{a}{2}[01\bar{1}]$ and $\frac{a}{2}[\bar{1}01]$ dislocations

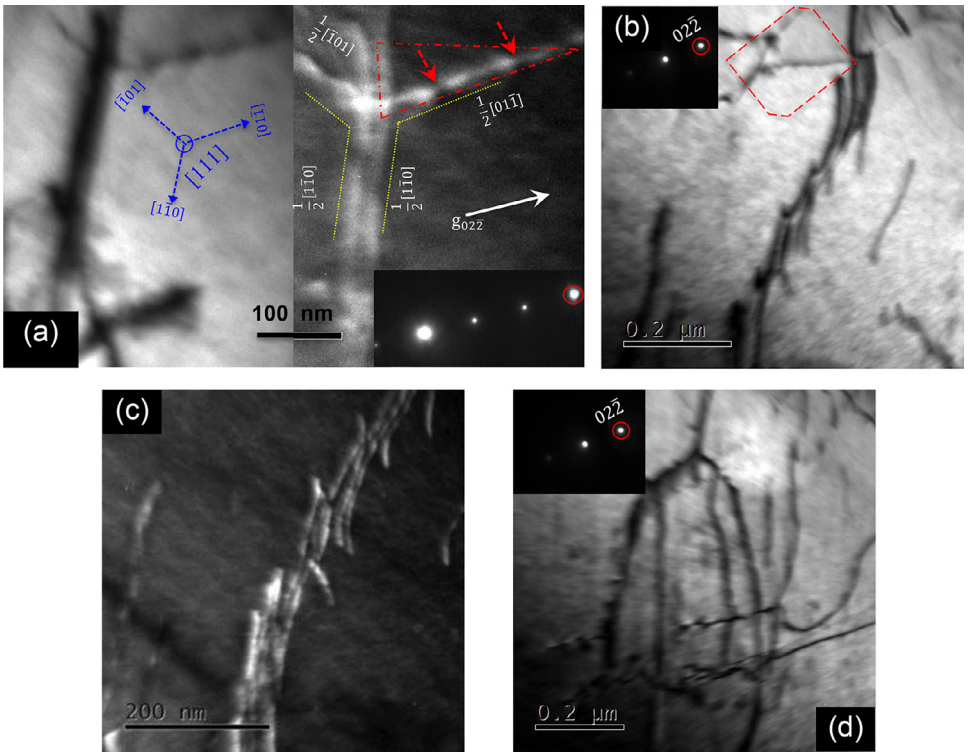

Fig. 2. Micrographs at 2% strain showing early dislocation activities: (a) high magnification BF and DF imaging in $B \approx [111]$ with strong and weak $g_{02\bar{2}}$ beam, respectively, showing impingement of pinned $\frac{a}{2}[01\bar{1}]$ and $\frac{a}{2}[\bar{1}01]$ screw dislocations with $\frac{a}{2}[1\bar{1}0]$ dipole dislocation. The dotted yellow segments on either side of the $\frac{a}{2}[1\bar{1}0]$ dipole will be jogged for impingement on parallel (111) planes. The unpinned segment having Burgers vector: $\frac{a}{2}[1\bar{1}0]$ would bow under the external stress to form a cross-slip loop string. (b) Formation of dislocation multipoles with strong $g_{02\bar{2}}$ beam. A truncated loop string is delineated using the red lines. (c) The corresponding weak beam image of (b). (d) The early stages of a Taylor lattice formation under two-beam BF condition in $B \approx [111]$.

having screw components and a $\frac{a}{2}[1\bar{1}0]$ dipole dislocation takes place on parallel (111) planes.

The corresponding weak beam dark field (WBDF) image in Fig. 2(a) under a g – 3 g diffraction condition in selected area diffraction (SAD) pattern inset, reveals that the dislocation segment having the Burgers vector $\frac{a}{2}[01\bar{1}]$ is showing a strong contrast and is also parallel to the $g_{02\bar{2}}$ diffraction vector. Hence, it is in a near screw orientation and pinned at the two points indicated by red arrows. In other words, it is locked in the screw direction, while the dipole segment (*i.e.* $\frac{a}{2}[1\bar{1}0]$) showing weaker contrast is predominantly edge in nature (the character angle between the diffraction vector and dislocation line, $\beta \sim 60°$) [18,20,21], bows under the action of the local stress field. Hence, a jog is formed on either side of the $\frac{a}{2}[1\bar{1}0]$ dipole dislocation, considering that the impingement of the two dislocations is on parallel slip planes (see legend in Fig. 2(a)). The locked dislocation ($\frac{a}{2}[01\bar{1}]$ or $\frac{a}{2}[\bar{1}01]$) prevents the pivot point from being trailed in the cross-slip plane under the tension exerted by the bowing dislocation (*i.e.* $\frac{a}{2}[1\bar{1}0]$ segment).

This would result in an L-shaped, hairpin like dislocation configuration along the moving dislocation, better known as prismatic loop strings formed through truncation of the dipole by coordinated cross-slip [22,23]. This mechanism, interpreted as cross-slip truncation (CST) mechanism, involves the impingement of two dislocations moving on parallel slip planes with different velocities such that they mutually annihilate by coordinated cross-slip [24]. These loop strings are usually only observed in some single crystals deformed in single slip involving $\frac{a}{2}\langle 110\rangle$ dislocations with screw components [24]: they have never been reported in high-Mn steels. A prismatic loop string forms when the red delineated region in Fig. 2(a) truncates from the initial jogged configuration through cross-slip. In agreement with this, the BF micrograph presented from a different grain in Fig. 2(b) shows a truncated loop string in the region outlined in red, which seemingly terminated from the jogged configuration seen in Fig. 2(a) [25] formed through the pinning of $\frac{a}{2}\langle 110\rangle$ screw dislocations [26]. Fig. 2(b) further shows a group of bowed dislocation multipoles under a strong $g_{02\bar{2}}$ reflection. The corresponding WBDF image depicted in Fig. 2(c) shows the near edge nature ($\beta \sim 70°$) of the dislocations constituting the multipoles. These multipoles align along the primary slip direction, and are formed by the cross-slip led juxtaposition of edge dislocations [27]. To our knowledge, Kim et al. [3] have reported only about the role of dislocation multipoles in the plasticity of high-Mn steels. They observed that such multipoles are created through successive cross-slip events and represent an energetically stable configuration.

Fig. 2(d) further exemplifies the situation in a new grain; wherein, the interaction of $\frac{a}{2}\langle 110\rangle$ dislocations via selective planar glide occurs on a single {111} plane. This glide of $\frac{a}{2}\langle 110\rangle$ dislocations is a consequence of the 'glide plane softening effect', arising from the short range ordering (SRO) induced by Al, resulting in well-known Taylor lattice formation [9]. A Taylor lattice forms at early strains as a result of pronounced planar glide on the most highly stressed glide planes without any systematic lattice rotations and/or also through alignment of cross-slip led edge components of the loop strings [28]. Taylor lattice and loop strings are low-energy dislocation structures (LEDS), whose contribution to strain hardening is still unclear [9,28].

A further implication of the WBDF image in Fig. 2 is that the individual $\frac{a}{2}\langle 110\rangle$ dislocations do not resolve into leading and trailing Shockley partials under weak beam diffraction conditions, which could have been utilized to measure the SFE of the steel, as adopted previously [18,19], while the $\frac{a}{2}[1\bar{1}0]$ dipole clearly splits into its constituent dislocations. The absence of dissociated $\frac{a}{2}\langle 110\rangle$ dislocations in Fig. 2 gives an indication that the dissociation is restricted due to a high SFE [29,30]. The sub-regular solution model of SFE in high-Mn steels predicts a SFE ~ 25 mJ/m^2 [31], and with this value, dissociated $\frac{a}{2}\langle 110\rangle$ dislocations should be omnipresent at low strains [18–20]. In the absence of dissociated $\frac{a}{2}\langle 110\rangle$ dislocations, the SFE (γ) of the steel was determined from X-ray analyses, based on the following equation utilizing the relationship between the SFE, stacking fault probability (P_{sf}), dislocation density (ρ) and lattice parameter (a), shown previously to be as effective as the TEM method, though indirect in nature [18].

$$\gamma = \frac{K_{111}\omega_0 G a A^{-0.37}}{\sqrt{3}\pi P_{sf}}\left\{\left(\frac{b}{2\pi}\right)^2\left(\pi\rho\bar{C}_{111}\right)\ln\left(\frac{R_e}{L}\right)\right\} \quad (1)$$

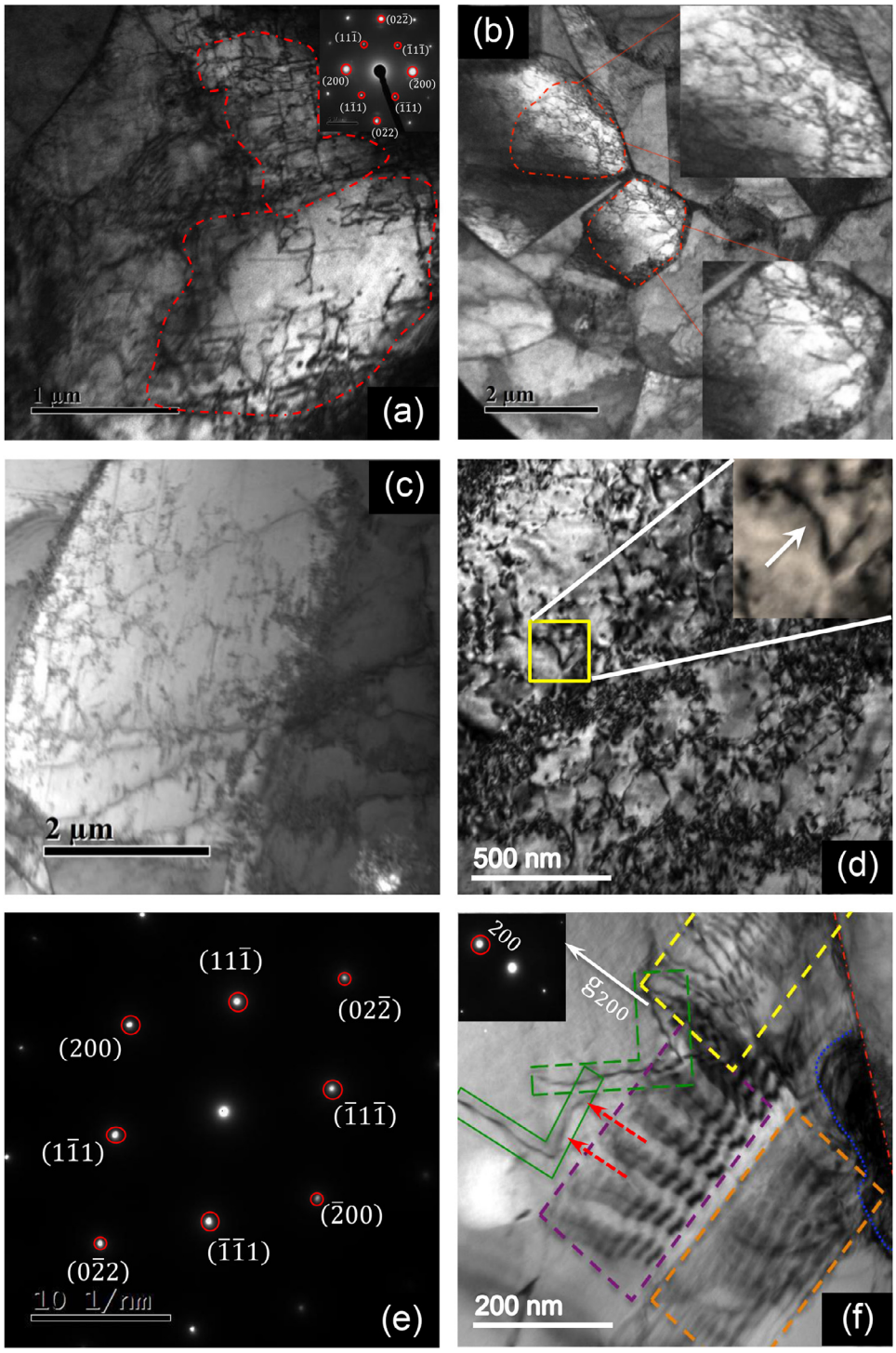

Fig. 3. BF micrographs of the specimen along showing: (a) extension of Taylor lattice to whole grain at 5% strain imaged along $B \approx [011]$ and delineated using red (b) weak dislocation cells at 10% strain at low magnification are delineated using red (c) high magnification image of weak dislocation cells in $B \approx [011]$ at 10% strain (d) a loop string amongst dislocation debris at failure strain ~ 50% under multi-beam conditions (e) diffraction condition of (d) in $B \approx [011]$ (f) a two-beam condition showing the nucleation and suppression of twinning at 10% strain. Please refer to the text for description to other legends.

Further parameters in Eq. (1) are magnitude of Burgers vector of perfect dislocations ($b = |\frac{a}{2}\langle 110\rangle|$), outer cut-off radius of the dislocation strain field (R_e) and Fourier variable (L). $A \sim 3.43$, is an anisotropy factor related to the X–ray elastic constants, $K_{111}\omega_0$ is proportionality constant ~ 6.6 [32] and $\bar{C}_{111}$ is the average contrast factor of dislocations for the Bragg reflection (111) of austenite. These descriptions are detailed elsewhere [33]. Eq. (1) yields the SFE ~ 60 mJ/m^2, which is significantly higher than the thermodynamic SFE of the steel (~ 25 mJ/m^2) that treats it as an intrinsic parameter. However, it is known that such a proposition is generally not applicable for high-Mn steels, wherein, the actual SFE is significantly modified by the local environment [18-20].

Fig. 3 presents an overview of the microstructure evolving at higher strain levels, including the fracture strain, while additional overview microstructure of the steel at various deformation levels are reported elsewhere [33]. The low magnification $B \approx [011]$ multi-beam image in Fig. 3(a) demonstrates the proliferation of Taylor lattices to the entire grain at 5% strain, while a further low magnification in Fig. 3(b) shows several austenite grains at 10% strain containing weakly developed dislocation cell substructures, *i.e.* transformation of planar to wavy slip.

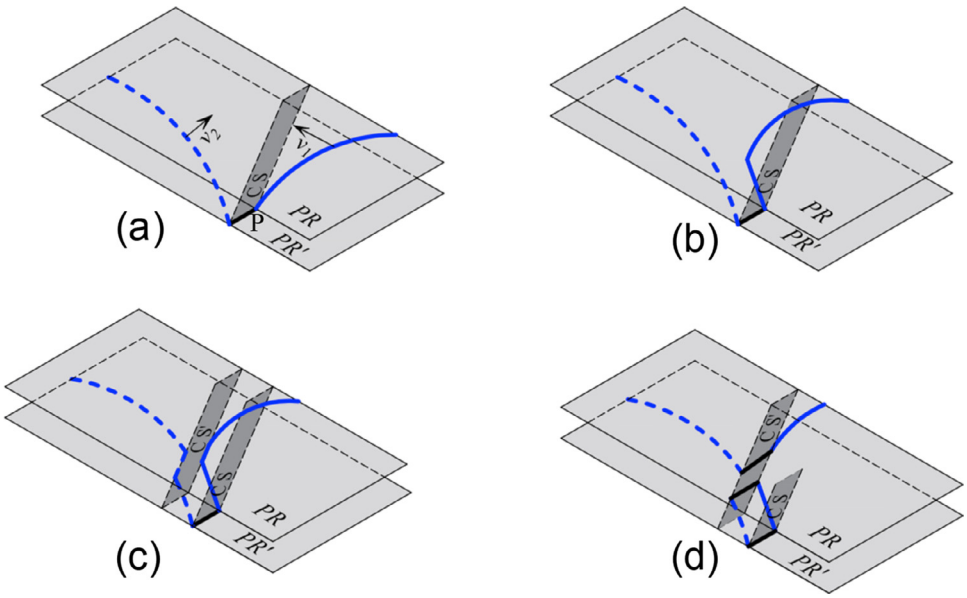

Fig. 4. The schematic of loop string formation in Fig. 2: (a) two impinging dislocations moving on parallel primary slip planes (PR and PR') with velocities v_1 and v_2 are jogged at P, $v_1 \gg v_2$. The jog (solid black segment) is free to move on the darkly shaded cross-slip plane (CS). (b) The dislocation segment in solid blue trails a hairpin like dipole configuration along the least mobile segment. (c) The two blue segments (solid and dashed) forming the dipole is aligned in the screw direction and cross-slips to the next parallel plane (CS'). (d) The glissile segments thus form the first loop through annihilation and this maneuver can repeat itself to produce several loops in succession.

Alongside, a high magnification multi beam $B \approx [011]$ image of weak dislocation cells at 10% strain is presented in Fig. 3(c). It is known that Taylor lattices can easily transform into dislocation cells and when glide on more than one plane takes place [28]. Fig. 3(d) reveals the copious dislocations debris observed in a specimen that failed at 50% strain, which interestingly possesses a pair of dislocation segments, indicated by the short arrow within the sepia inset, whose selected area diffraction pattern is shown in Fig. 3(e). Veyssiére and Grègori indirectly made a conclusion that such L or V-shaped dislocation segments arise from termination of the loop strings by a closing jog and their subsequent relaxation towards edge orientation [25]. Such a configuration of the loop string was first observed in the studied steel at the onset of deformation (Fig. 2), and thus the proposition of Veyssiére and Grègori [25] seems to be tenable in the present study. Kubin and Devincre [34] further suggested that the configurations of these loop strings remain stable under deformation, as also observed here.

Nevertheless, as an opposing observation, no sign of deformation twinning was observed until fracture [18,35]. Therefore, it is postulated that twinning is suppressed in the steel, while the plasticity is mediated by concomitant dislocation substructures produced through successive cross-slip. In an attempt to clarify the reason for twinning suppression in the steel, we present a two-beam BF micrograph in Fig. 3(f), which was obtained with g_{200} along $B \approx [011]$ from a grain of the 10% strained specimen containing relatively low density of defects. It nicely illustrates the reason for twin suppression in a single frame. Two distinct loop strings are again observed within the green regions (Fig. 3(f)), whose mobile segments bow under the action of the local stress field (the bowing direction indicated by a pair of red dashed arrows), which is in agreement with the WBDF micrograph in Fig. 2(a). Other regions delineated using different colors reveal important observations, which are now discussed. The grain boundary shown using a long dashed red line emits perfect dislocations, which are piled up on the primary slip plane (yellow region). Alongside, a region of high dislocation density in the form of dislocation forest/tangles (delineated by the blue line) is also discernible in Fig. 3(f).

Interestingly, the dislocation proliferations delineated by blue and yellow lines in Fig. 3(f) have had different implications on the microstructure evolution of the steel. For instance, twin nucleation is observed within the purple region, through overlapping stacking faults (SFs), revealing periodic contrast of the Shockley twinning partials, as reported recently [13,18,19]. SFs in this steel remained uncharacteristically absent, otherwise. Further, the dislocations piled up within the yellow region are expected to be perfect, since they do not reveal any fringe contrast, unlike the dislocations within the twinned region. Therefore, it is justifiable that the stress field associated with this sporadic pile-up (within yellow region) provides the nucleation stress for the fitful occurrence of twinning in Fig. 3(f) [5]. On the other hand, the region demarcated by blue line, owing to its high local dislocation density would also possess a high local stress field, ruptures the regular arrangement of SFs within the orange outlined region. Consequently, any twinning opportunity is terminated. It is recently reported that presence of any dislocation stress field in the matrix is not conducive for observing twinning [36]. In other words, this reaffirms the postulate of Boucher and Christian [37] that presence of dislocation substructure in the matrix would strongly suppress any deformation twinning activity.

Finally, the high SFE of the steel $\sim$ 60 mJ/m^2, determined by Eq. (1) is to be interpreted as effective SFE, essentially arising due to suppression of SF formation induced by grain boundary induced back-stress [8]. In this situation, twinning is largely suppressed since the classical twinning routes are not activated under high SFE conditions [38], and the plasticity is carried out by several LEDS produced through successive cross-slip operations. Kubin and Devincre [34] proposed that these LEDS are impenetrable obstacles, which cause strain hardening by delaying dynamic recovery in stage C, without any significant lowering in SHR. This situation is quite different from the normal high SFE fcc alloys without LEDS, wherein, stress-assisted cross-slip promotes dynamic recovery (*i.e.* reduced strain hardening), which was not observed here. The mechanism of loop string formation in the present steel is schematically presented in Fig. 4.

To summarize, quasi-static uniaxial tensile deformation of a fine-grained ($\sim$ 5 μm) Fe-Mn-Al-C steel reveals nearly uniform high strain hardening rate $\sim$ 2 GPa, associated with dislocation mediated plasticity and concomitant suppression of twinning. Plasticity was governed by a cross-slip assisted dislocation truncation mechanism producing dislocation loop strings and Taylor lattices at early strain. Such a cross-slip based mechanism is expected to delay dynamic recovery in stage C to produce a good combination of high strength and ductility.

Declaration of Competing Interest

The authors declare that they have no known competing financial interests or personal relationships that could influence the work reported in this paper.

Acknowledgements

SRD acknowledges Department of Science and Technology, Government of India, DST/Inspire fellowship (Grant no. IF1706172). SS recognizes the support of UGC-JRF scheme of Government of India (Grant no. 521511). JIK, DP and LPK express their gratitude to the Academy of Finland, Genome of Steel (Profi3) through project #311934. PCC and PS acknowledge the Department of Science and Technology, Government of India, for financial support received under the framework of Science & Engineering Research Board (SERB) grant number: CRG/2019/000858.

References

[1] Z.C. Luo, M.X. Huang, Revisit the role of deformation twins on the work-hardening behavior of twinning-induced plasticity steels, Scr. Mater. 142 (2018) 28–31.
[2] X. Fu, X. Wu, Q. Yu, Dislocation plasticity reigns in a traditional twinning-induced plasticity steel by in situ observation, Mater. Today Nano. 3 (2018) 48–53.
[3] S.-D. Kim, J.Y. Park, S.-J. Park, J. Hoon Jang, J. Moon, H.-Y. Ha, C.-H. Lee, J.-Y. Kang, J.-H. Shin, T.-H. Lee, Direct observation of dislocation plasticity in high--Mn lightweight steel by in-situ TEM, Sci. Rep. 9 (2019) 1–13 15171.
[4] J.K. Kim, B.C. De Cooman, Stacking fault energy and deformation mechanism in Fe-xMn-0.6C-yAl TWIP steel, Mater. Sci. Eng. A 676 (2016) 216–231.
[5] B.C. De Cooman, Y. Estrin, S.K. Kim, Twinning-induced plasticity (TWIP) steels, Acta Mater 142 (2018) 283–362.
[6] P. Volosevich, V. Gridnev, Y. Petrov, Influence of Mn and the stacking fault energy of Fe-Mn alloys, Phys. Met. Metallogr. 42 (1976) 126–130.
[7] S. Takaki, H. Nakatsu, Y. Tokunaga, Effects of austenite grain size on ε-martensitic transformation in Fe-15 mass% Mn alloy, Mater. Trans. JIM 34 (1993) 489–495.
[8] Y.-K. Lee, C. Choi, Driving force for γ/ε martensitic transformation and stacking fault energy of γ in Fe-Mn binary system, Metall. Mater. Trans. A 31 (2000) 355–360.
[9] K.-T. Park, Tensile deformation of low-density Fe-Mn-Al-C austenitic steels at ambient temperature, Scr. Mater. 68 (2013) 375–379.
[10] E. Welsch, D. Ponge, S.M. Hafez Haghighat, S. Sandlobes, P. Choi, M. Herbig, S. Zaefferer, D. Raabe, Strain hardening by dynamic slip band refinement in a high-Mn lightweight steel, Acta Mater 116 (2016) 188–199.
[11] D. Hull, D.J. Bacon, Introduction to Dislocations, Fifth Edition, Butterworth-Heinemann, Oxford, 2011.
[12] P.B. Hirsch: The Physics of Metals, P. B. Hirsch (Ed.), Cambridge University Press, Cambridge, 1975.
[13] L.P. Kubin, J. Kratochvíl, Elastic model for the sweeping of dipolar loops, Philos. Mag. A 80 (2000) 201–218.
[14] R. Ueji, N. Tsuchida, D. Terada, N. Tsuji, Y. Tanaka, A. Takemura, K. Kunishige, Tensile properties and twinning behavior of high manganese austenitic steel with fine-grained structure, Scr. Mater. 59 (2008) 963–966.
[15] J.-E. Jin, Y.-K. Lee, Strain hardening behavior of a Fe-18Mn-0.6C-1.5Al TWIP steel, Mater. Sci. Eng. A 527 (2009) 157–161.
[16] J.-E. Jin, Y.-K. Lee, Effects of Al on microstructure and tensile properties of C- bearing high Mn TWIP steel, Acta Mater 60 (2012) 1680–1688.
[17] W.J. Tunstall, P.J. Goodhew, Electron microscope image contrast of double loops in quenched aluminium, Philos. Mag. 13 (1966) 1259–1272.
[18] B. Mahato, S.K. Shee, T. Sahu, S. Ghosh Chowdhury, P. Sahu, D.A. Porter, L.P. Karjalainen, An effective stacking fault energy viewpoint on the formation of extended defects and their contribution to strain hardening in Fe-Mn-Si-Al twinning induced plasticity steel, Acta Mater 86 (2015) 69–79.
[19] B. Mahato, T. Sahu, S.K. Shee, P. Sahu, T. Sawaguchi, J. Kömi, L.P. Karjalainen, Simultaneous twinning nucleation mechanisms in an Fe-Mn-Si-Al twinning induced plasticity steel, Acta Mater 132 (2017) 264–275.
[20] D.T. Pierce, J.A. Jiménez, J. Bentley, D. Raabe, C. Oskay, J.E. Wittig, The influence of manganese content on the stacking fault and austenite/ε-martensite interfacial energies in Fe-Mn-(Al-Si) steels investigated by experimental and theory, Acta Mater 68 (2014) 238–253.
[21] G. Laplanche, A. Kostka, C. Reinhart, J. Hunfeld, G. Eggeler, E.P. George, Reasons for the superior mechanical properties of medium-entropy CrCoNi compared to high--entropy CrMnFeCoNi, Acta Mater 128 (2017) 292–303.
[22] J.W. Steeds, Dislocation arrangement in copper single crystals as a function of strain, Proc. R. Soc. A 292 (1966) 343–373.
[23] X. Shi, G. Saada, P. Veyssière, The annihilation of superdislocations in Ni3Al during deformation at room temperature, Philos. Mag. Lett. 71 (1995) 1–9.
[24] P. Veyssière, F. Grégori, Properties of {110}{111} slip in Al-rich γ-TiAl deformed at room temperature III. The role of loop strings in the pinning and the patterning of dislocations, Philos. Mag. A 82 (2002) 579–590.
[25] P. Veyssière, F. Grégori, Properties of {110} (111} slip in Al-rich γ-TiAl deformed at room temperature II. The formation of strings of prismatic loops, Philos. Mag. A 82 (2002) 567–577.
[26] D. Caillard, M. Legros, A. Couret, Extrinsic obstacles and loop formation in deformed metals and alloys, Philos. Mag. 93 (2013) 203–221.
[27] P.J. Jackson, The role of cross-slip in the plastic deformation of crystals, Mater. Sci. Eng. 57 (1983) 39–47.
[28] D. Kuhlmann-Wilsdorf, Theory of Plastic Deformation:- properties of low energy dislocation structures, Mater. Sci. Eng. A ll3 (1989) 1–41.
[29] I.L.F Ray, D.J.H. Cockayne, Investigation of dislocation geometries in the diamond cubic structure, J. Microsc. 98 (1973) 170–173.
[30] D.J.H. Cockayne, M.L. Jenkins, I.L.F. Ray, The measurement of stacking-fault energies of pure face-centred cubic metals, Philos. Mag. 24 (1971) 1383–1392 192.
[31] A. Saeed-Akbari, J. Imlau, U. Prahl, W. Bleck, Derivation and Variation in Composition-Dependent Stacking Fault Energy Maps Based on Subregular Solution Model in High-Manganese Steels, Metall. Mater. Trans. A 40 (2009) 3076–3090.
[32] S. Martin, S. Wolf, U. Martin, L. Krüger, D. Rafaja, Deformation Mechanisms in Austenitic TRIP/TWIP Steel as a Function of Temperature, Metal. Mater. Trans. A 47 (2016) 49–58.
[33] S.R. Das, S. Shyamal, S.K. Shee, J.I. Kömi, P. Sahu, X-ray line profile analysis of the deformation microstructure in a medium-grained Fe-Mn-Al-C austenitic steel, Mater. Charact. 172 (2021) 110833.
[34] L.P. Kubin, B. Devincre, et al., From dislocation mechanisms to dislocation microstructures and strain hardening, in: Bilde-Sørensen, et al. (Eds.), Deformation Induced Microstructures: Analysis and Relation to Properties, Risø National Laboratory, Roskilde, Denmark, 1999, pp. 61–83.
[35] H. Idrissi, K. Renard, L. Ryelandt, D. Schryvers, P.J. Jacques, On the mechanism of twin formation in Fe-Mn-C TWIP steels, Acta Mater 58 (2010) 2464–2476.
[36] S. Shyamal, M. Ghiasabadi Farahani, T. Allam, A.S. Hamada, C. Haase, J.I. Kömi, P.C. Chakraborti, P. Sahu, Activation of a hybrid twinning mechanism in a Cr-Ni-Si-V-N medium manganese austenitic steel containing precipitates, Scr. Mater. 192 (2021) 83–88.
[37] N.A. Boucher, J.W. Christian, The influence of pre-strain on deformation twinning in niobium single crystals, Acta Metall 20 (1972) 581–591.
[38] M.G. Farahani, A. Zarei-Hanzaki, H.R. Abedi, J.H. Kim, M. Jaskari, P. Sahu, L.P. Karjalainen, On the activation of alternated stacking fault pair twinning mechanism in a very large-grained Fe-29Mn-2.4Al steel, Scr. Mater. 178 (2020) 301–306.